NRC Research Press

ARTICLE

A density functional theory and spectroscopic study of intramolecular quenching of metal-to-ligand charge-transfer excited states in some monobipyridine ruthenium(II) complexes

Shivnath Mazumder, Ryan A. Thomas, Richard L. Lord, H. Bernhard Schlegel, and John F. Endicott

Abstract: The complexes $[Ru(NCCH_3)_4bpy]^{2+}$ and $[Ru([14]aneS_4)bpy]^{2+}$ ([14]aneS$_4$ = 1,4,8,11-tetrathiacyclotetradecane, bpy = 2,2′-bipyridine) have similar absorption and emission spectra but the 77 K metal-to-ligand charge-transfer (MLCT) excited state emission lifetime of the latter is less than 0.3% that of the former. Density functional theory modeling of the lowest energy triplet excited states indicates that triplet metal centered (^{3}MC) excited states are about 3500 cm^{-1} lower in energy than their ^{3}MLCT excited states in both complexes. The differences in excited state lifetimes arise from a much larger coordination sphere distortion for $[Ru(NCCH_3)_4bpy]^{2+}$ and the associated larger reorganizational barrier for intramolecular electron transfer. The smaller ruthenium ligand distortions of the $[Ru([14]aneS_4)bpy]^{2+}$ complex are apparently a consequence of stereochemical constraints imposed by the macrocyclic[14]aneS$_4$ ligand, and the ^{3}MC excited state calculated for the unconstrained $[Ru(S(CH_3)_2)_4bpy]^{2+}$ complex ($S(CH_3)_2$ = dimethyl sulfide) is distorted in a manner similar to that of $[Ru(NCCH_3)_4bpy]^{2+}$. Despite the lower energy calculated for its ^{3}MC than ^{3}MLCT excited state, $[Ru(NCCH_3)_4bpy]^{2+}$ emits strongly in 77 K glasses with an emission quantum yield of 0.47. The emission is biphasic with about a 1 μs lifetime for its dominant (86%) emission component. The 405 nm excitation used in these studies results in a significant amount of photodecomposition in the 77 K glasses. This is a temperature-dependent biphotonic process that most likely involves the bipyridine-radical anionic moiety of the ^{3}MLCT excited state. A smaller than expected value found for the radiative rate constant is consistent with a lower energy ^{3}MC than ^{3}MLCT state.

Key words: density functional theory modeled ruthenium triplet excited states, metal-centered excited state quenching of charge-transfer emission.

Résumé : Les complexes $[Ru(NCCH_3)_4bpy]^{2+}$ et $[Ru([14]aneS_4)bpy]^{2+}$ ([14]aneS$_4$ = 1,4,8,11-tétrathiacyclotétradécane, bpy = 2,2′-bipyridine) présentent des spectres d'absorption et d'émission similaires, mais le temps de vie d'émission de l'état excité du transfert de charge du métal vers le ligand (« metal-to-ligand charge transfer » ou MLCT) à 77 K du second complexe est égal à moins de 0,3 % de celui du premier. La modélisation par la théorie de la fonctionnelle de la densité des états triplets excités de plus basse énergie montre que les états triplets excités centrés sur le métal (^{3}MC) possèdent une énergie environ 3500 cm^{-1} inférieure à celle de leurs états excités ^{3}MLCT dans le cas des deux complexes. Les différences entre les temps de vie des états excités proviennent d'une distorsion beaucoup plus importante de la sphère de coordination dans le complexe $[Ru(NCCH_3)_4bpy]^{2+}$ et de la plus grande barrière de réorganisation du transfert électronique intramoléculaire qui l'accompagne. Les moins grandes distorsions ruthénium ligand du complexe $[Ru([14]aneS_4)bpy]^{2+}$ sont apparemment une conséquence des contraintes stéréochimiques imposées par le ligand macrocyclique [14]aneS$_4$. Par ailleurs, l'état excité ^{3}MC calculé dans le cas du complexe $[Ru(S(CH_3)_2)_4bpy]^{2+}$ non soumis à des contraintes ($S(CH_3)_2$ = sulfure de diméthyle) est distordu d'une manière semblable à celle du complexe $[Ru(NCCH_3)_4bpy]^{2+}$. Malgré une plus basse énergie calculée pour son état ^{3}MC que pour son état excité ^{3}MLCT, le complexe $[Ru(NCCH_3)_4bpy]^{2+}$ émet fortement dans des verres à 77 K, avec un rendement quantique d'émission de 0,47. L'émission est biphasique avec un temps de vie d'environ 1 μs pour son composant d'émission majoritaire (86 %). L'excitation à 405 nm utilisée dans les présentes études entraîne une importante photodécomposition dans les verres à 77 K. Il s'agit d'un processus biphotonique dépendant de la température qui implique très vraisemblablement la moitié anionique du radical pyridine de l'état excité ^{3}MLCT. La valeur de la constante de taux d'émission mesurée inférieure à celle attendue est en adéquation avec l'énergie de l'état ^{3}MC elle-même inférieure à celle de l'état ^{3}MLCT. [Traduit par la Rédaction]

Mots-clés : états triplets excités du ruthénium modélisés à l'aide de la théorie de la fonctionnelle de la densité, désactivation de l'état excité centré sur le métal de l'émission de transfert de charge.

Introduction

Intramolecular excited-state electron-transfer processes are often key components of schemes for photocatalysis and solar energy conversion. Such processes mediated by excited states of transition metal complexes have been of particular interest for some time due to the strong visible region absorptivities of their ground states.[1–12] Electron transfer rates depend predominantly on the molecular energy and structural and solvational differences between the reactants and products,[7,13–19] with electronic factors contributing under some circumstances.[17,18,20–24] Electron transfers from vibrationally relaxed excited states of these complexes depend on these same parameters, but they are compli-

Received 25 March 2014. Accepted 2 June 2014.

S. Mazumder, R.A. Thomas, H.B. Schlegel, and J.F. Endicott. Department of Chemistry, Wayne State University, Detroit, MI 48202, USA.
R.L. Lord. Grand Valley State University, 1 Campus Dr., Allendale, MI 49401-9403, USA.
Corresponding authors: H. Bernhard Schlegel (e-mail: hbs@chem.wayne.edu) and John F. Endicott (e-mail: jfe@chem.wayne.edu).
This article is part of a Special Issue dedicated to Professor Barry Lever in recognition of his contributions to inorganic chemistry across Canada and beyond.

cated by difficulties in determining them, since the excited state lifetimes of transition metal complexes are too short for the methods that are standard for the characterization of molecular ground states. Thus, the reaction-driving forces are usually based on the assumption that the reaction proceeds from the lowest energy excited state and transition metal excited-state structures are most often inferred from more indirect methods such as resonance Raman spectra,[25–28] modeling based on the vibronic side bands found in low temperature emission spectra,[29–31] density functional theory (DFT) modeling,[32] and transient X-ray absorption methods.[33] Complications can arise in the determination of the structure–reactivity relations for transition metal complex excited states because (*i*) their reactions usually involve a change of spin multiplicity at the metal center, (*ii*) excited-state electron-transfer processes must be fast and sometimes compete with excited-state vibrational relaxation, and (*iii*) there can be many excited states, with different electronic configurations and nuclear geometries in the energy range between the Franck–Condon states initially populated by light absorption and the lowest energy excited states that are believed to be responsible for most of the observed photochemical properties. The complications introduced by this energy proximity of different excited states in transition metal complexes can involve[34,35] (*i*) differences in the electronic configurations and molecular structures of the Franck–Condon and lowest energy excited states, (*ii*) a variety of possible molecular relaxation channels of the Franck–Condon states, and (*iii*) thermally activated internal conversion among these states. Recent advances in computational approaches have permitted the relatively accurate modeling of transition metal complex electronic states with high spin multiplicities.[32,34,36–53]

In this paper, we have used DFT approaches to model excited-state electronic and nuclear structures and the energy constraints on intramolecular excited-state ligand-to-metal electron transfer for some Ru-bpy complexes whose lowest energy metal-to-ligand charge-transfer (MLCT) excited states emit at the highest energies known for this class of chromophores. Thus, we recently reported that $[Ru(NCCH_3)_4bpy]^{2+}$ and $[Ru([14]aneS_4)bpy]^{2+}$ both emit in the 15 000–20 000 cm^{-1} region and that their emission spectra have very similar vibronic envelopes. However, the 77 K emission lifetime of the latter is orders of magnitude shorter than that of the former,[32] and this may implicate efficient quenching of the ^{3}MLCT excited state of $[Ru([14]aneS_4)bpy]^{2+}$ by a lower energy ^{3}MC state (see Fig. 1). The $[Ru(NCCH_3)_4bpy]^{2+}$ emission lifetime at 77 K is comparable with that of $[Ru(bpy)_3]^{2+}$, but its ambient quantum yield for the photosubstitution of acetonitrile by water has been reported to be about 0.43.[54] This has been interpreted in terms of mediation by a highly distorted metal-centered triplet excited state, ^{3}MC, whose energy is comparable with or slightly higher than that of the lowest energy ^{3}MLCT excited state.[54] If the lowest energy triplet excited state were the ^{3}MC state, then one might expect either an anomalously short lifetime such as that reported for $[Ru([14]aneS_4)bpy]^{2+}$[32] or small quantum yield for the emitting state as found for $[Ru(L)_4MDA]^{m+}$ complexes (MDA is a monodentate aromatic ligand).[34] Although no photosubstitution quantum yield has been reported for $[Ru([14]aneS_4)bpy]^{2+}$, this complex is not difficult to handle in ambient light[32,55] and its photosubstitution yield is very likely smaller than that of $[Ru(NCCH_3)_4bpy]^{2+}$. In this paper, we report on the DFT modeling of the lowest energy ^{3}MLCT excited state of this complex to gain insight into these contrasts in photochemistry and photophysics and we report a more critical evaluation of its unusually complex emission properties.

Experimental

DFT procedures

Electronic structure calculations were carried out using DFT[56] as implemented in a developmental version of Gaussian[57] with the B3PW91 functional[58,59] and SDD basis set and pseudopotential[60–62] on the metal and 6-31G(d) basis[63,64] on the lighter atoms. Wave functions were tested for SCF stability and all of the optimized structures were confirmed as minima by analyzing the harmonic vibrational frequencies. The ground-state singlet and triplet dication states were computed with standard SCF methods, and analytic frequencies were obtained for each. Solvation effects (in acetonitrile) were accounted for using the implicit SMD continuum solvation model[65] and were included during structure optimization. The isodensity plots of the orbitals involved in these transitions were visualized using GaussView.[66] The Seam.nb Mathematica notebook[67] was used to find a minimum on a seam of intersection between ^{3}MLCT and ^{3}MC triplet potential energy surfaces using a Lagrangian multiplier approach.

Fig. 1. Qualitative potential energy curves illustrating the possible energy relationships between the ^{1}MLCT, ^{3}MLCT, and ^{3}MC excited states of a simple donor–acceptor system. Note that the distortions of the excited states are generally in many nuclear vibrational modes and that distortion modes of the MC states are very different from those of the MLCT excited states so the relationships of the potential energy surfaces are more complex than indicated in this figure.

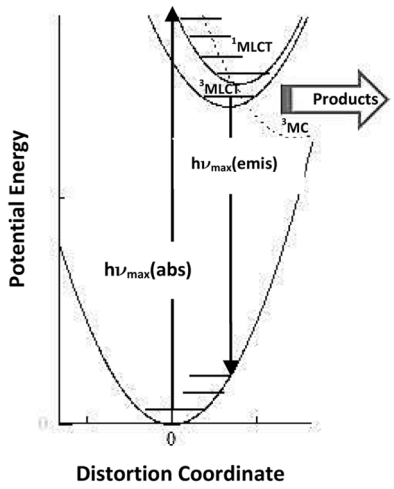

Compounds employed

The following commercial chemicals were used with no further purification: 2,2′-bipyridine (bpy), acetonitrile ($NCCH_3$), and NH_4PF_6. The syntheses of $[Ru([14]aneS_4)bpy]^{2+}$[32,55] and $[Ru(NCCH_3)_4bpy]^{2+}$[54,68] have been previously reported. Complexes employed were characterized using electrochemical and NMR techniques and only preparations with no indication of impurity contributions were used in this study.

Instrumentation

UV-vis absorption spectra at ambient temperature were determined using a Shimadzu spectrophotometer UV-2101PC. Low-temperature (90 K) UV-vis spectra were determined in ethanol–methanol (4:1, *v*/*v*) glasses using xenon emission lines for wavelength calibration and a NIST traceable Oriel model 63358 QTH lamp for intensity. A QTH lamp was used as the light source for low-temperature spectroscopic measurements. An Oxford Instruments OptistatCF static exchange gas continuous-flow cryostat with liquid nitrogen as the cryogen was used at 90 K with NSG Precision Cells, Inc. cryogenic square 1 cm quartz cuvettes. A gradual temperature decrease from ambient temperature to 90 K was employed to minimize solvent-glass cracking and quartz cuvette fracturing. The detection system was an ANDOR Shamrock 500 spectrometer with dual exit ports and equipped with a 600 l/mm, 500 nm blaze grating. An ANDOR Newton DU920-BV detector head was mounted on the exit ports of the Shamrock 500 spectrometer and cooled to –90 °C. Light was collected with a lens and transmitted by means of Thorlabs

3 mm Core Liquid Light Guide LLG0338-4 (wavelength range 340–800 nm) to an Andor F/# matcher SR500i to the spectrometer's entrance slit. Emission lifetimes were determined using Spectra Physics 337205-00 nitrogen laser-pumped dye laser system for excitation and a Jobin-Yvon H-10 spectrometer for detection with PMT output digitized using a PC with a National Instruments NI PCI-5154, 2 GS/s, 1 GHz digitizer w/8 MB/ch onboard memory PC card.

Emission procedures

Complexes were irradiated in their MLCT absorption bands using a 405 nm (50 mW) CW diode laser module purchased from Power Technologies, Inc. (Little Rock, Arkansas) or using a Spectra Physics nitrogen laser-pumped dye laser-pulsed system. Wavelength calibration and light collection and transmission were achieved with the same setup as described in the instrumentation section. The 77 K emissionsampleswerepreparedin2mmcylindricalcellsinbutyronitrile or ethanol–methanol (4:1, *v*/*v*) immersed in liquid N_2 in a Dewar as previously described.[29] The calibrated spectral emission intensities were generated in units of photons per second.[69] All samples were deareated for 10 min with argon at ambient temperature prior to emission and lifetime measurements.

Quantum yield procedures

The emission quantum yield of $\Phi_R = 0.376$ (±0.036)[70] for $[Ru(bpy)_3]^{2+}$ in 77 K ethanol–methanol glasses was used as the reference for relative emission yield determinations in this study. Equation 1 was used to calculate the relative quantum yield of the target sample complexes (Φ_S):[70]

$$\frac{\Phi_S}{\Phi_R} = \frac{I_S}{I_R}\frac{1 - 10^{-A_R}}{1 - 10^{-A_S}}\frac{\eta_S^2}{\eta_R^2} \quad (1)$$

where I_S and I_R are the integrated areas of the emission spectral curves of the sample complex and the reference, respectively, A_S and A_R are the absorbances at the excitation wavelength, and η is the refractive index of the solvent system. When the solvent is the same for the reference and the target sample, then $\eta_S^2/\eta_R^2 = 1$.

The photodecomposition quantum yield at 77 K was determined using a 405 nm (50 mW) CW diode laser module for excitation. After an initial emission spectrum was obtained at 77 K, the sample was further irradiated for a period of time (typically 3 or 6 min). Subsequent emission spectra were collected in 3 and 6 min intervals over a total range of 21 min. This method was also used in conjunction with neutral density filters in front of the laser to vary the radiation intensity.

Results and discussion

Although the $[Ru([14]aneS_4)bpy]^{2+}$ and $[Ru(NCCH_3)_4bpy]^{2+}$ complexes differ appreciably in their photosensitivity and 77 K emission yields and lifetimes, their ambient absorption spectra and 77 K emission spectra are very similar.[32] The computational modeling of the present work indicates that the lowest energy excited state of each of these complexes is a triplet metal-centered, ^{3}MC, excited state with the ^{3}MLCT excited state higher in energy by a few thousand wavenumbers. However, the distortions of the lowest energy ^{3}MC state are smaller for the former compound than for the latter and it is largely this feature that leads to the contrasts in photochemistry and photophysics.

Computational modeling

$[Ru([14]aneS_4)bpy]^{2+}$

The tetrathiamacrocyclic ligand in the $[Ru([14]aneS_4)bpy]^{2+}$ complex, **1**, can potentially give rise to different conformational isomers resulting from the lone-pair inversion of the coordinated sulfur atoms. Figure 2 depicts the optimized geometries and computed relative energies of three possible different ground-state conformational isomers, **1A**, **1B**, and **1C**, for complex **1**. These isomers differ in the way the lone pairs of the sulfur atoms are orientated. Isomer **1A**, with one sulfur lone pair in an *endo* configuration and the other one in the *exo* position, is found to be lower in energy than the others by 2450–3550 cm^{-1}. The Ru–S bond distances are found to be similar (2.341 and 2.355 Å for Ru–S_{eq} and 2.377 Å for Ru–S_{ax}) and the Ru–N(bpy) distances are 2.117 and 2.123 Å in isomer **1A**. These calculated structural parameters are in good agreement with those determined in the X-ray crystal structure.[55]

The computational modeling indicates that there are two ^{3}MC excited states with similarly low energies for $[Ru([14]aneS_4)bpy]^{2+}$: T_0 and T_1 have spin densities on ruthenium of 1.60 and 1.70, respectively, compared with the spin density of 0.86 calculated for ruthenium in the ^{3}MLCT excited state (T_2) (see Fig. 3). Variations of the metal–ligand bond distances and the relevant bond angles calculated for these states are shown in Table 1. The Ru–S bond lengths are calculated to be 2.303–2.401 Å, while the Ru–N(bpy) bond distances are 2.105 and 2.121 Å in the ^{3}MLCT state. Both of the ^{3}MC states are more highly distorted than the ^{3}MLCT excited state. The T_1 state is distorted along the N_2(bpy)–Ru–S_1 axis with Ru–N_2(bpy) and Ru–S_1 bond lengths of 2.487 and 2.553 Å, respectively, and hence, significantly elongated compared with those found in the charge-transfer state (2.121 and 2.342 Å). The T_0 state is distorted in the N_1–S_4–S_2–S_3 plane with all of the bond lengths in this plane being longer than those in either the ^{3}MLCT or the ground state (see Fig. 4 for ligand numbering scheme). This effect is most prominent for the Ru–S_3 and Ru–S_2 bonds, which are elongated by 0.358 and 0.288 Å, respectively, relative to the charge-transfer state T_2. The bond angles N_1–Ru–S_4 and S_3–Ru–S_2 are also affected as a result of the change in the bond distances. The former angle increases significantly from 90.18° in the T_2 state to 119.85° in the T_0 state, while the S_3–Ru–S_2 angle decreases from 83.82° in the charge-transfer state to 73.01° in the metal-centered state. The distortions of T_0 are reminiscent of the distortions inferred for the lowest energy triplet metal-centered states from high-resolution absorption spectra of $[Co(NH_3)_6]^{3+}$[71] and emission spectra of $[Rh(NH_3)_6]^{3+}$.[72] However, the metal-centered excited-state distortions of $[Ru([14]aneS_4)bpy]^{2+}$ do not map neatly into those of the octahedral complexes, since isomer **1A** of the tetrathiaether complex has much lower symmetry (C_1) and the N_1–S_4–S_2–S_3 and N_2–S_4–S_2–S_1 planes are not equivalent.

$[Ru(NCCH_3)_4bpy]^{2+}$

The DFT-optimized lowest energy triplet metal-to-ligand charge-transfer (^{3}MLCT) and metal-centered (^{3}MC) excited states of the $[Ru(NCCH_3)_4bpy]^{2+}$ complex are shown in Fig. 5 and Table 1 lists the calculated coordination sphere bond lengths. The axial Ru–N_{axial}(acetonitrile) bond lengths calculated for the ^{3}MC molecular structure are considerably longer, 2.519 and 2.614 Å, than those calculated for the ^{3}MLCT state, 2.020 and 2.021 Å. Thus, the ^{3}MC state is axially distorted with respect to both the ^{3}MLCT and the ground state. The Mulliken spin densities calculated on ruthenium are 0.73 and 1.93 for the ^{3}MLCT and ^{3}MC states, respectively.

Isosurface plots of the Ru-d orbital occupation in the singlet ground (S_0) and triplet excited states (T_1 and T_0) of the $[Ru(NCCH_3)_4bpy]^{2+}$ complex are depicted in Fig. 6. The HOMO (dπ3) calculated in the S_0 state is a combination of the d_{xz} and d_{yz} orbitals on ruthenium. Thus, the charge-transfer state (T_1) is a result of an electron promotion from this orbital into a π* orbital of bpy (Fig. 7). The metal-centered state T_0 involves an electron transfer from the dπ3 into the d_{z2} orbital on ruthenium, and as a result, it is axially distorted. This distortion (about 0.5 Å per Ru–N bond for S_0/T_0) is much larger than the comparable distortion (about 0.3 Å per Ru–S bond for S_0/T_0) calculated for the $[Ru([14]aneS_4)bpy]^{2+}$ complex, and the minimum found on the potential energy surface for the $[Ru(NCCH_3)_4bpy]^{2+}$ complex is much

Fig. 2. DFT-computed optimized geometries and relative energies ($cm^{-1}/10^3$) of three isomers of the $[Ru([14]aneS_4)(bpy)]^{2+}$ complex. Hydrogen atoms are omitted for clarity.

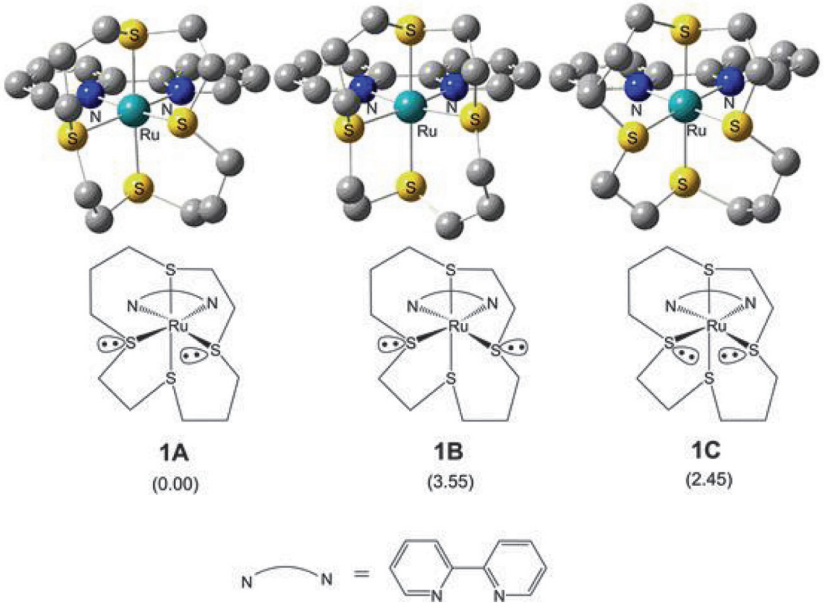

Fig. 3. DFT-optimized structures and spin density plots of the T_2, T_1, and T_0 states of the $[Ru([14]aneS_4)(bpy)]^{2+}$ complex.

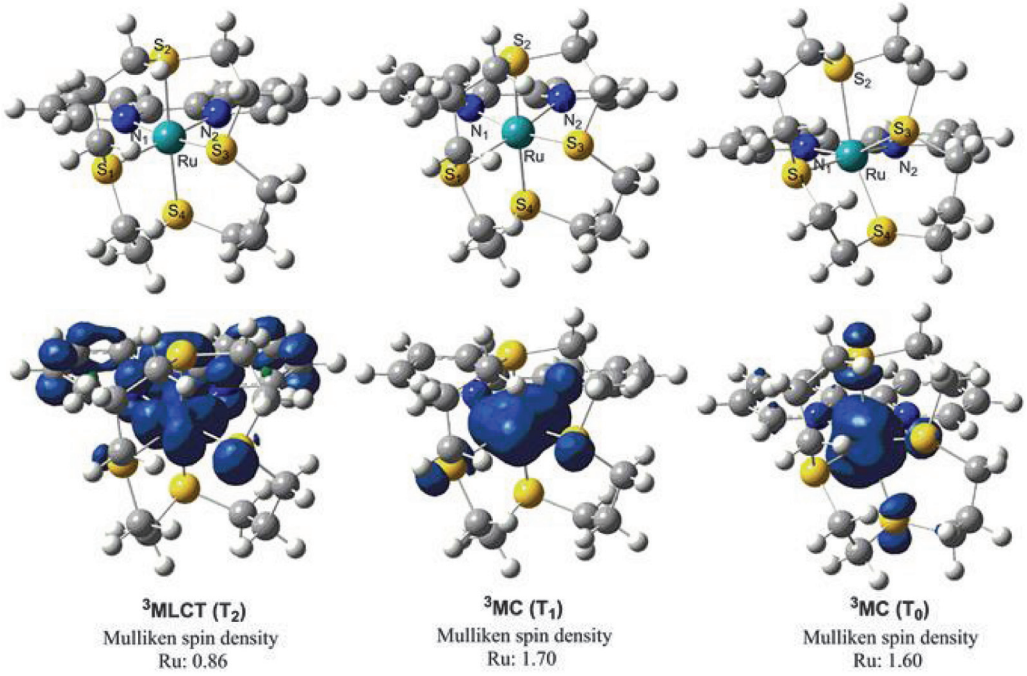

more shallow. Comparison of the d-orbital population between the S_0 states of the $[Ru(NCCH_3)_4bpy]^{2+}$ (Fig. 6) and $[Ru([14]aneS_4)bpy]^{2+}$ (Fig. 8) complexes demonstrate that unlike the former complex, the HOMO for $[Ru([14]aneS_4)bpy]^{2+}$ species is a d_{xy} orbital on ruthenium (Fig. 8) and the ^{3}MLCT state involves transfer of an electron from this orbital into the π^* orbital of bpy. Interestingly, the donor orbital for this ^{3}MLCT state has an appreciable amount of character at S_3 that suggests a redox noninnocent role of the tetrathiamacrocycle in this excited state.

Photophysical implications of the DFT modeling

As illustrated in Fig. 9, the ^{3}MC state is lower in energy than the ^{3}MLCT state by about 3850 cm^{-1} for the complex $[Ru(NCCH_3)_4bpy]^{2+}$. The major differences between the molecular structures of these two states are the lengths of the Ru–N_{axial}(acetonitrile) bonds, which are elongated by 0.499 and 0.593 Å in the ^{3}MC state compared with those in the ^{3}MLCT state. The elongation of those bonds leads to a significant reorganizational energy for the conversion of the charge-transfer state to the metal-centered state and a large difference in the nuclear coordinates for potential energy minima of the two states. Consequently, one would expect an appreciable energy barrier for the crossing between them (see Fig. 9). The seam of the intersection between the charge-transfer and metal-centered potential energy surfaces was calculated (see supporting information for details in the Supplementary material

Table 1. Comparison of Ru–L and Ru–N(bpy) bond lengths (Å) and relevant bond angles (°) calculated for the T_2, T_1, and T_0 states of the $[Ru(L)_4bpy]^{2+}$ complexes.

Ancillary ligand, L	State	Relative energy[a]	Ru–L_1	Ru–L_2	Ru–L_3	Ru–L_4	Ru–N_1	Ru–N_2	∠L_2–Ru–L_3	∠N_1–Ru–L_4
[14]aneS$_4$/4	T_2(MLCT)	20.0	2.342	2.401	2.303	2.389	2.105	2.121	83.82	90.18
	T_1(MC)	16.6	2.553	2.366	2.328	2.383	2.248	2.487	83.09	90.41
	T_0(MC)	16.4	2.360	2.689	2.661	2.471	2.145	2.099	73.01	119.85
	S_0	0.0	2.341	2.377	2.355	2.377	2.117	2.123	82.97	90.90
$NCCH_3$	T_1(MLCT)	21.0	2.073	2.020	2.073	2.021	2.014	2.014	90.38	89.68
	T_0(MC)	17.2	2.077	2.519	2.065	2.614	2.070	2.067	94.16	92.96
	S_0	0.0	2.040	2.018	2.039	2.018	2.065	2.065	90.17	89.89
$(CH_3)_2S$	T_1(MLCT)	18.8	2.470	2.415	2.474	2.429	2.087	2.034	90.49	90.12
	T_0(MC)	14.4	2.431	2.888	2.438	2.939	2.112	2.105	89.01	88.53
	S_0	0.0	2.423	2.432	2.430	2.388	2.105	2.097	92.15	93.01

[a] ΔE(SCF), $cm^{-1}/10^{-3}$.

Fig. 4. Coordination sphere numbering scheme for the $[Ru(L)_4bpy]^{2+}$ complexes.

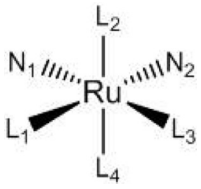

Fig. 5. DFT-optimized structures and spin density plots of the T_1 and T_0 states of the $[Ru(CH_3CN)_4(bpy)]^{2+}$ complex.

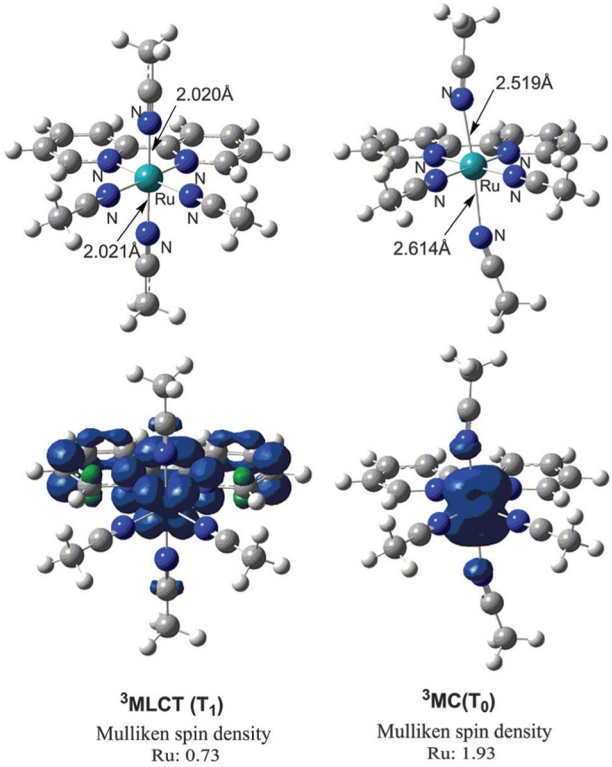

section), and the minimum crossing point, $\mathbf{X_1}$, is found to be 1910 cm^{-1} (≈36 k_BT at 77 K) higher in energy than the ^{3}MLCT potential energy minimum. This is a relatively deep local or upper state potential energy minimum and therefore, a thermally activated ^{3}MLCT → ^{3}MC internal-conversion process is not expected to compete with the nonradiative and radiative decay rates characteristic of a Ru-bpy ^{3}MLCT excited state in this energy range.

The computed geometry of $\mathbf{X_1}$ is shown in Fig. 10. The axial Ru–N_2(acetonitrile) and Ru–N_4(acetonitrile) bond lengths for the system at the crossing point are 2.148 and 2.147 Å, respectively, which are longer than in the ^{3}MLCT state and shorter than in the ^{3}MC state. Variations of the calculated bond lengths of the bpy ligand as a result of conversion of the ^{3}MLCT to $\mathbf{X_1}$ to the ^{3}MC state are shown in Table 2. The C_1–$C_{1'}$ and C_2–C_3 bond lengths of the bpy ligand are 1.404 and 1.368 Å, respectively, in the ^{3}MLCT state, while they are longer, 1.465 and 1.390 Å, respectively, in the ^{3}MC state. In contrast, the C_1–C_2, C_3–C_4, and N–C_1 bond lengths decrease from the charge-transfer state to the metal-centered state. Scarborough and Wieghardt have noted that the π* orbital of bpy (Fig. 7) that accommodates the electron in the charge-transfer state is bonding in C_1–$C_{1'}$ and C_2–C_3 while antibonding in C_1–C_2, C_3–C_4, and N–C_1 and proposed that the change in the C_1–$C_{1'}$ length of bpy of the transition metal–bpy complex is proportional to the amount of the charge on the bpy ligand.[52] The C_1–$C_{1'}$, C_1–C_2, C_2–C_3, C_3–C_4, and N–C_1 bond distances in the intersection point $\mathbf{X_1}$ are found to be intermediate between those of the charge-transfer and metal-centered states.

The metal-centered states T_1 and T_0 are found to be lower in energy by 3450 and 3620 cm^{-1}, respectively, than the charge-transfer state T_2 for the $[Ru([14]aneS_4)bpy]^{2+}$ complex (Fig. 11). The Ru–N_2 and Ru–S_1 bond lengths are larger by 0.366 and 0.211 Å, respectively, in T_1 than in the ^{3}MLCT state, while the Ru–S_2 and Ru–S_3 bonds are larger by 0.358 and 0.288 Å, respectively, in T_0 than in the ^{3}MLCT state (Table 1). All of these displacements are considerably smaller compared with those (0.499 and 0.593 Å) found in the $[Ru(NCCH_3)_4bpy]^{2+}$ complex. Thus, the surface crossing model discussed above suggests that the intersection points $\mathbf{Y_1}$ and $\mathbf{Y_2}$ between the charge-transfer and metal-centered potential energy surfaces for the $[Ru([14]aneS_4)bpy]^{2+}$ complex will be located nearer the ^{3}MLCT potential energy minimum than is $\mathbf{X_1}$ for the $[Ru(NCCH_3)_4bpy]^{2+}$ complex. To examine this hypothesis, scans of the potential energy surface were performed along the Ru–S_3 and Ru–S_1 bonds (Fig. 12). For each case, the scan was started with the optimized geometry of the ^{3}MLCT state and the Ru–S bond distance was changed at every step with an increment of 0.01 Å. The spin densities on ruthenium were monitored to ensure convergence to the right electronic states (see supporting information for details). At every point of the scan, the Ru–S bond length was fixed, while a full geometry optimization was done on the rest of the molecule. As demonstrated in those figures, the ^{3}MLCT state is very unstable with respect to its conversion to the ^{3}MC state and the energy requirement for this transformation is below 180 cm^{-1}. Scanning of the potential energy surface along the C_1–$C_{1'}$ bond of the bpy ligand (Fig. 12*c*) also demonstrates the spontaneous transformation of the charge-transfer state to the metal-centered state. These results, the relatively small coordination sphere displacements, and the surface crossing model discussed above suggest that $\mathbf{Y_1}$ and $\mathbf{Y_2}$ are near the potential energy

rich2/ccj-cjc/ccj-cjc/ccj99914/ccj0335d14z | xppws | S=3 | 7/31/14 | 11:32 | 4/Color Fig: F2-F3,F5-F14,F16 | Art: cjc-2014-0155 | Input-1st disk, 2nd ?
Pagination not final (cite DOI) / Pagination provisoire (citer le DOI)

Fig. 6. Isosurface plots (0.05 au) of the Ru-d orbital population in the S_0, T_1 (^{3}MLCT), and T_0 (^{3}MC) states of the $[Ru(NCCH_3)_4(bpy)]^{2+}$ complex.

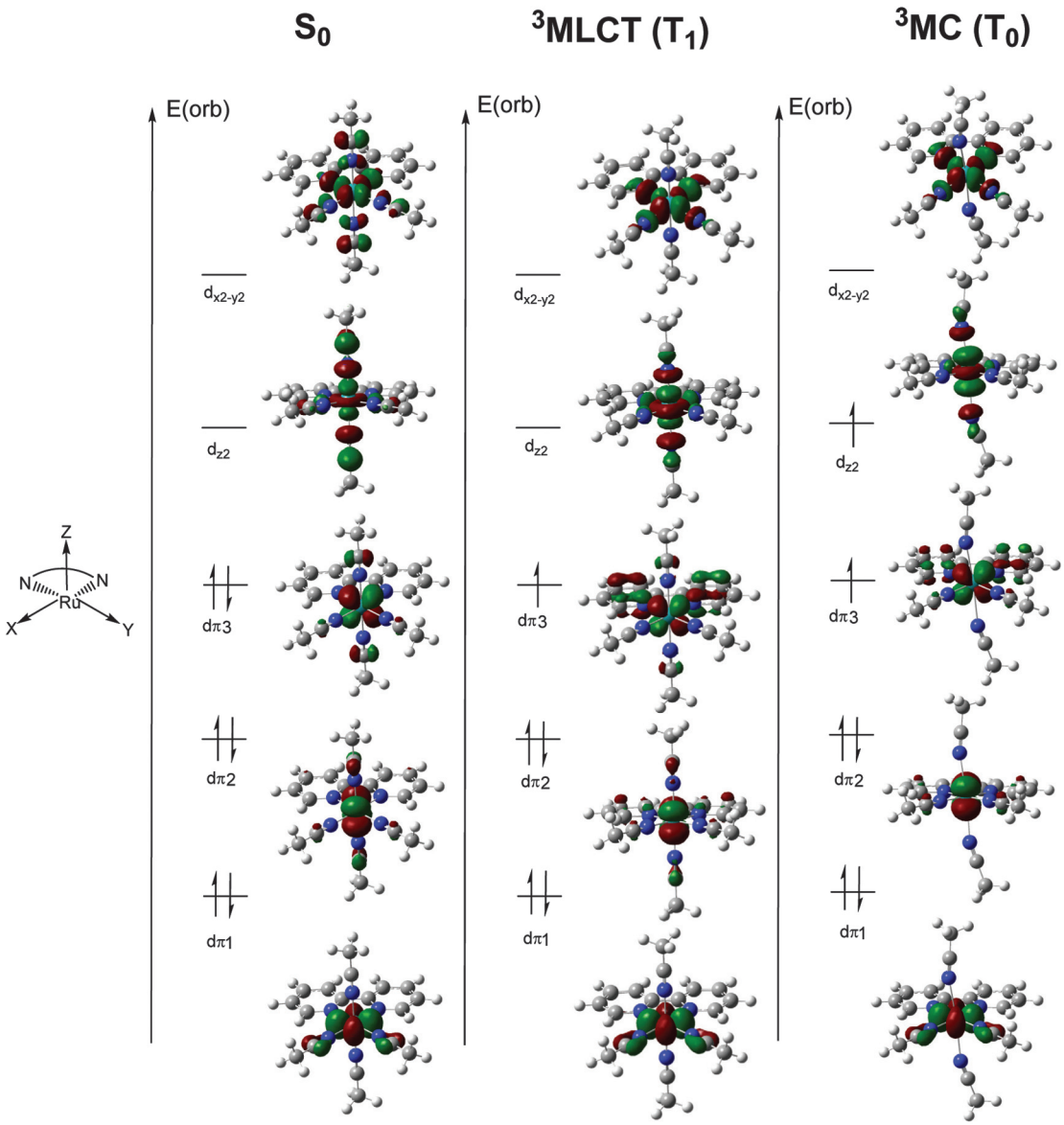

Fig. 7. Isosurface plot (0.05 au) of the bpy-π* orbital that is populated in the T_1 (^{3}MLCT) state of the $[Ru(NCCH_3)_4(bpy)]^{2+}$ complex.

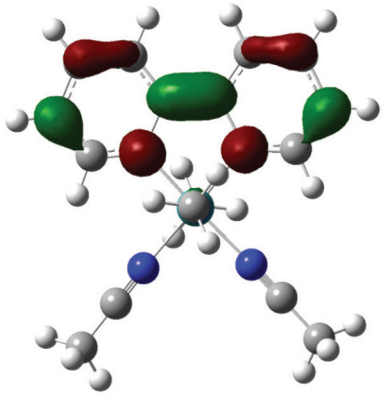

F13

minimum of the ^{3}MLCT state (Fig. 11), but their values could not be optimized due to the very small energies involved. The very small barrier (<3 k_BT at 77 K) for a thermally activated ^{3}MLCT → ^{3}MC internal-conversion process for the $[Ru([14]aneS_4)bpy]^{2+}$ complex is consistent with the much weaker emission and shorter lifetime of its ^{3}MLCT excited state than that of the $[Ru(NCCH_3)_4bpy]^{2+}$ complex.

It is likely that the noted contrasts in the size of the coordination sphere displacements and the resulting excited state stabilities calculated for the $[Ru([14]aneS_4)bpy]^{2+}$ and $[Ru(NCCH_3)_4bpy]^{2+}$ complexes have their origin in stereochemical constraints introduced by the[14]$aneS_4$ ligand. To examine this hypothesis, we have examined computationally the relatively simple model $[Ru(SMe_2)_4bpy]^{2+}$ complex in which the thiaether ligands are less constrained. Figure 13 illustrates the molecular geometries along with the spin density plots of the charge-transfer and metal-centered states of the complex $[Ru(SMe_2)_4bpy]^{2+}$. Interestingly, the ^{3}MC state of this complex is found to be axially distorted (S_2–Ru–S_4), which contrasts with the distortions of the T_0 and T_1 states of presence of the $[Ru([14]aneS_4)bpy]^{2+}$ complex. The ^{3}MC state of $[Ru(SMe_2)_4bpy]^{2+}$ is lower in energy than the ^{3}MLCT state by

Fig. 8. Isosurface plots (0.05 au) of the Ru-d orbital population in the S_0 and T_2 (^{3}MLCT) states of the [Ru([14]aneS$_4$)(bpy)]$^{2+}$ complex. See supporting information for the Ru-d orbital population of the T_1 and T_2 states.

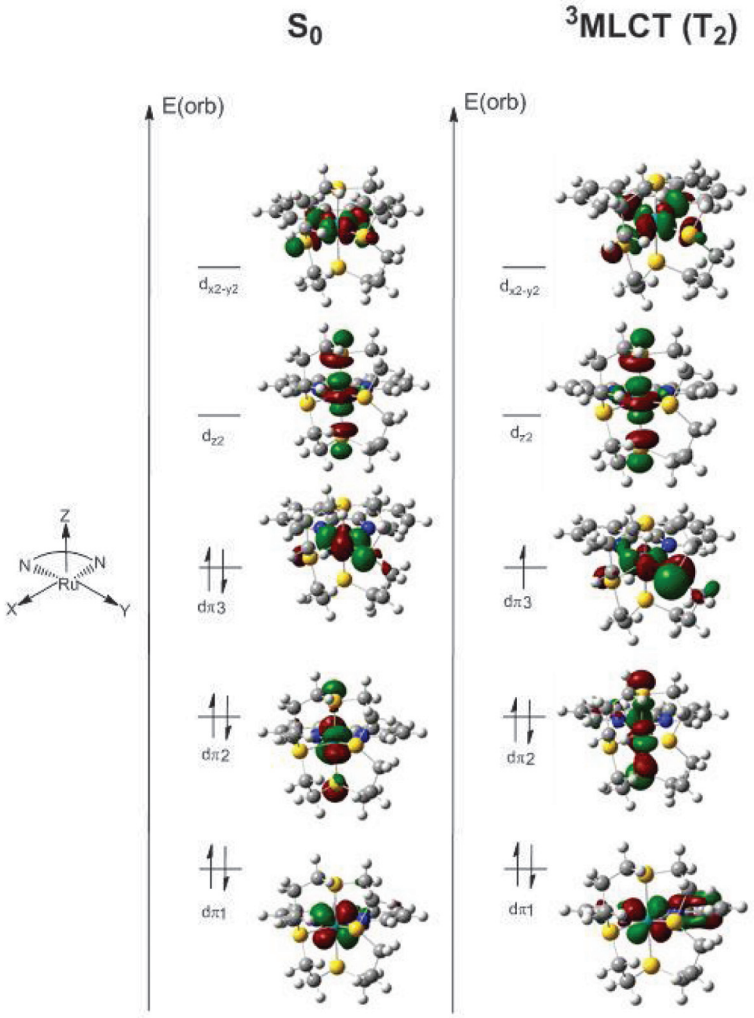

4400 cm^{-1}. The Ru–S_{axial} bonds of this state, 2.888 and 2.939 Å, are significantly elongated (by 0.473 and 0.510 Å) compared with the ^{3}MLCT state. The distortions of the Ru–S bonds are larger in this complex than those found for the [Ru([14]aneS$_4$)bpy]$^{2+}$ complex (0.358, 0.288, 0.366, and 0.211 Å), a feature that can be attributed to the stereochemical constraints imposed by the macrocyclic ligand of the latter.

Photochemistry and photophysics of [Ru(NCCH$_3$)$_4$bpy]$^{2+}$

The [Ru(NCCH$_3$)$_4$bpy]$^{2+}$ complex emits very strongly in glasses at 77 K. Thus, we find an emission quantum yield (0.47 ± 0.04) in 4:1 ethanol–methanol glasses, which is larger than that of [Ru(bpy)$_3$]$^{2+}$ (0.37).[70] However, the spectroscopic and quantum yield determinations were complicated by (*i*) substrate photodecomposition induced by extended periods of irradiation and (or) the use of high-intensity diode laser excitation and (*ii*) complex emission decay kinetics. Within our experience, these features of the excited-state behavior of the [Ru(NCCH$_3$)$_4$bpy]$^{2+}$ complex are very unusual for ruthenium–bipyridine complexes in 77 K glasses and they complicate the experimental characterization of the ^{3}MLCT excited state for this complex.

The 77 K photodecomposition of [Ru(NCCH$_3$)$_4$bpy]$^{2+}$

Irradiations of [Ru(NCCH$_3$)$_4$bpy]$^{2+}$ at 405 nm with a 50 mW diode laser for several minutes result in appreciable changes in the emission spectra as shown in Fig. 14.

The photo-induced spectral changes most likely correspond to the substitution of an acetonitrile ligand by a solvent species, since irradiation results in the decrease in amplitudes of all emission bands of [Ru(NCCH$_3$)$_4$bpy]$^{2+}$ (Fig. 14), while in butyronitrile, there are shifts and changes in the relative intensities of these emission bands. These observations are consistent with the expectation that the substitution by an alcohol should result in a lower energy ^{3}MLCT excited state, while substitution by butyronitrile results in a complex whose emission is in the same general spectral region. The amount of photodecomposition(s) tends to decrease with the duration of the irradiation, which suggests second-order photolysis and (or) photo-product filter effects. We have used the emission spectral changes to estimate the photodecomposition quantum yields in 77 K ethanol–methanol glasses.

The quantum yield for photodecomposition, ϕ_{pd}, of a substrate S may be defined by

$$(2) \qquad \frac{d[S]}{dt} = -\phi_{pd} I_a$$

where I_a is the intensity of light absorbed (s^{-1}) and it can be defined by

$$(3) \qquad \phi_{em} = \frac{N_{em}}{N_a}$$

Fig. 9. Relative energetics of the ^{3}MLCT and ^{3}MC states on the triplet potential energy surface of the $[Ru(NCCH_3)_4bpy]^{2+}$ complex. The minimum found on the potential energy surface of the ^{3}MC state is very shallow and it is 3900 cm^{-1} lower in energy than that of the ^{3}MLCT state; X_1 denotes the minimum energy crossing point between the two states.

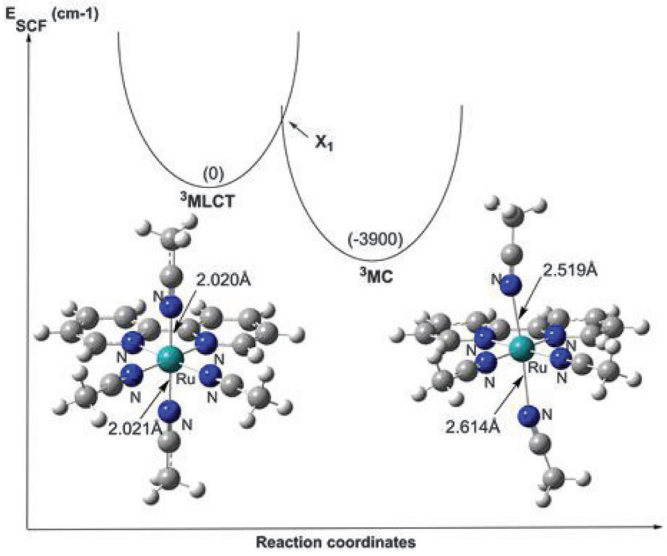

Fig. 10. Computed geometry of the minimum energy crossing point X_1 between the lowest ^{3}MLCT and ^{3}MC excited states for the $[Ru(NCCH_3)_4bpy]^{2+}$ complex.

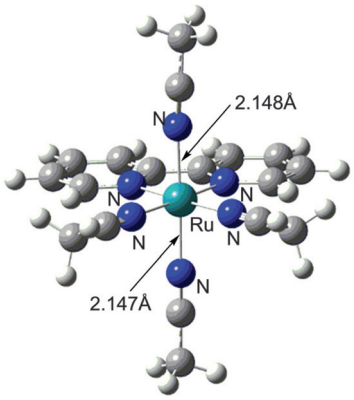

$$I_a = N_a \times \Delta t_a;\ I_{em} = N_{em} \times (\Delta t_a + \delta t_{em}) \quad (4)$$

where ϕ_{em} is the emission quantum yield, N_{em} is the number of photons of light emitted (s^{-1}), N_a is the number of photons of light absorbed (s^{-1}), Δt_a is the time interval for spectral accumulation, and δt_{em} is an effective for excited-state lifetime. In our experiments, Δt_a is on the order of several minutes, while δt_{em} is of the order of microseconds. Therefore:

$$I_a \approx \frac{I_{em}}{\phi_{em}} \quad (5)$$

$$\frac{d[S]}{dt} = -\phi_{pd} I_{em}/\phi_{em} \quad (6)$$

The total irradiation time is given by

Table 2. Comparison of the bond distances (Å) of bpy calculated for the ^{3}MLCT, ^{3}MC, and the minimum energy crossing point X_1 of the $[Ru(NCCH_3)_4bpy]^{2+}$ complex.

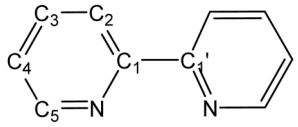

	C_1–$C_{1'}$	C_1–C_2	C_2–C_3	C_3–C_4	C_4–C_5	C_5–N	N–C_1
^{3}MLCT(T_1)	1.404	1.426	1.368	1.425	1.376	1.350	1.405
^{3}MC(T_0)	1.465	1.394	1.390	1.393	1.388	1.344	1.361
X_1	1.424	1.414	1.375	1.414	1.379	1.350	1.389

$$t_{rad} = [\text{time for spectral accumulation, } \Delta t_{sa}] + [\text{irradiation interval, } \Delta t_{ii}] \approx 0.5\Delta t_{sa} + \sum_{j=0} (j\Delta t_{ii} + 0.5j\Delta t_{sa}) \quad (7)$$

for the j number of times the sample was irradiated. Thus:

$$\phi_{pd} \approx [\Delta I_{em}(j) \times \Delta t_{sa} \times \phi_{em}]/[I_{em}(av)_j \times t_{rad}(j)] \quad (8)$$

where $I_{em}(av)_j = [I_{em}(j-1) + I_{em}(j)]/2$ and $\Delta I_{em}(j) = [I_{em}(j-1) - I_{em}(j)]$. The relative substrate emission intensity is calculated from $I_{rel} = I_{em}(j)/[\phi_{em} I_{em}(j=0)]$, where $\phi_{em} = 0.47$ (see discussion below).

The photodecomposition quantum yields, summarized in Fig. 15, clearly show that the photodecomposition yield (expressed as ϕ_{pd}) decreases strongly with radiation intensity as expected for a two-photon process. It also appears that photo-product absorption or other problems interfere with the long-time irradiations. Within the experimental uncertainties and in view of the fact that we have not used small enough values of I_o/n to establish an irradiation intensity independent region for photodecomposition, ϕ_{pd}(apparent) is approximately proportional to the intensity of radiation in the range I_o–$0.1I_o$. Based on these observations, we estimate $\phi_{pd} < 0.0002$ for the quantum yield of the primary photoproducts (if any) in the 77 K glass. This is of course a net decomposition quantum yield and not likely to be representative of the quantum yield for the primary Ru–$NCCH_3$ bond-breaking event (from a dissociative potential energy surface), since cage recombination must be far more important than product separation in a 77 K glass. F15

The two-photon photochemistry is most likely to be a consequence of the irradiation of the transient ^{3}MLCT excited state, since the bpy radical anion moiety in these complexes has an intense absorption at about 390 nm and the low-energy tail of this band would have reasonable intensity at 405 nm.[73] This situation is described by the following equations:

$$[(L)_4Ru^{II}(bpy)]^{2+} + h\nu_{405} \rightarrow {}^1\{\text{FC state}\} \rightarrow {}^3[(L)_4Ru^{III}(bpy^{-\cdot})]^{2+} \quad (9)$$

$$[(L)_4Ru^{III}(bpy^{-\cdot})]^{2+} \rightarrow [(L)_4Ru^{II}(bpy)]^{2+}, (k_r + k_{nr}) \quad (10)$$

$$[(L)_4Ru^{III}(bpy^{-\cdot})]^{2+} h\nu_{405} \rightarrow \text{products}, k_{pd} \quad (11)$$

For the 77 K excited state behavior of this complex represented by eqs. 9–11, $k_{obs} = (k_r + k_{nr} + k_{pd})$.

Low-temperature emission lifetimes of $[Ru(NCCH_3)_4bpy]^{2+}$

The emission decay of this complex at 77 K does not fit a single exponential. However, the emission decay data can be fitted by two components very well with only random residuals (Fig. 16), but a multicomponent decay cannot be rigorously ruled out. At 77 K, the two emission decay components had very nearly the same F16

Fig. 11. Relative energetics of the ^{3}MLCT and ^{3}MC states on the triplet potential energy surface of the [Ru([14]aneS$_4$)bpy]$^{2+}$ complex. The minima found on the potential energy surface of the ^{3}MC states are bound and 3500 and 3600 cm^{-1} lower in energy than that of the ^{3}MLCT state: Y_1 and Y_2 denote the minimum energy crossing points between those states.

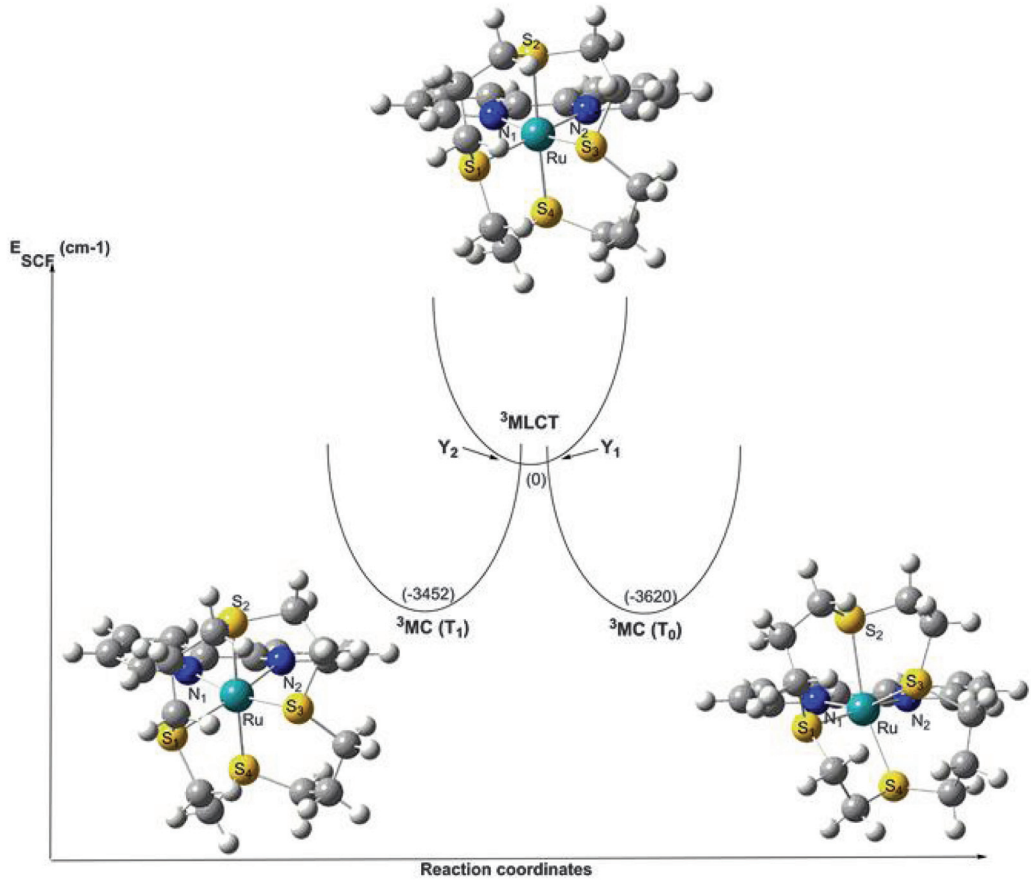

Fig. 12. Energetics of the relaxed scan along the bonds of the [Ru([14]aneS$_4$)bpy]$^{2+}$ complex. (*a*) Ru–S$_3$ (from a distance of 2.401 to 2.611 Å with an increment of 0.01 Å); (*b*) Ru–S$_1$ (from a distance of 2.341 to 2.551 Å with an increment of 0.01 Å); (*c*) C$_1$–C$_{1'}$ bond of bpy (from a distance of 1.415 to 1.495 Å with an increment of 0.01 Å). See supporting information for details.

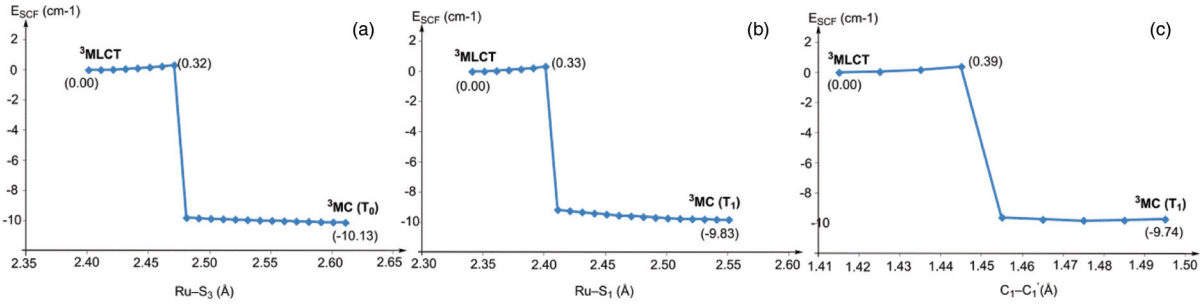

amplitudes (±5%) independent of the excitation (375–415 nm), monitoring wavelengths (510–600 nm), or solvent (alcohol or butyronitrile) (see Tables 3 and 4). However, the slower decay component makes the dominant contribution (≥80%) to the 77 K emission spectra, where the relative contribution of this decay component is determined by

$$\text{Fraction of contribution 2} = \frac{\int (A2)e^{-t/\tau(2)}dt}{\int (A2)e^{-t/\tau(2)}dt + \int (A1)e^{-t/\tau(1)}dt} = \frac{(A2)(\tau 2)}{(A2)(\tau 2) + (A1)(\tau 1)} \quad (12)$$

The [Ru(NCCH$_3$)$_4$bpy]$^{2+}$ emission decay rates are somewhat temperature dependent between 77 and 107 K (Table 5). This is complicated by the photochemical effects described above, since the spectral bandshape changes increase as the temperature increases. To determine how or whether the photochemical effects described above affect the lifetime and amplitude determinations, we examined the temperature dependence of the emission decay with and without intermediate photochemical irradiation periods and by varying the cryostat cooling sequence as follows.

(*i*) The experiments summarized at the top of Table 4 were performed for conditions that lead to significant photodecomposition. The lifetimes were determined at the specified temperature in the cryostat using 390 nm pulsed laser excitation and then

Fig. 13. Relative energetics of the ^{3}MLCT and ^{3}MC states on the triplet potential energy surface along with their spin density plots for the complex $[Ru(Me_2S)_4bpy]^{2+}$ complex. The minimum found on the potential energy surface of the ^{3}MC state is very shallow and it is 4400 cm^{-1} lower in energy than that of the ^{3}MLCT state.

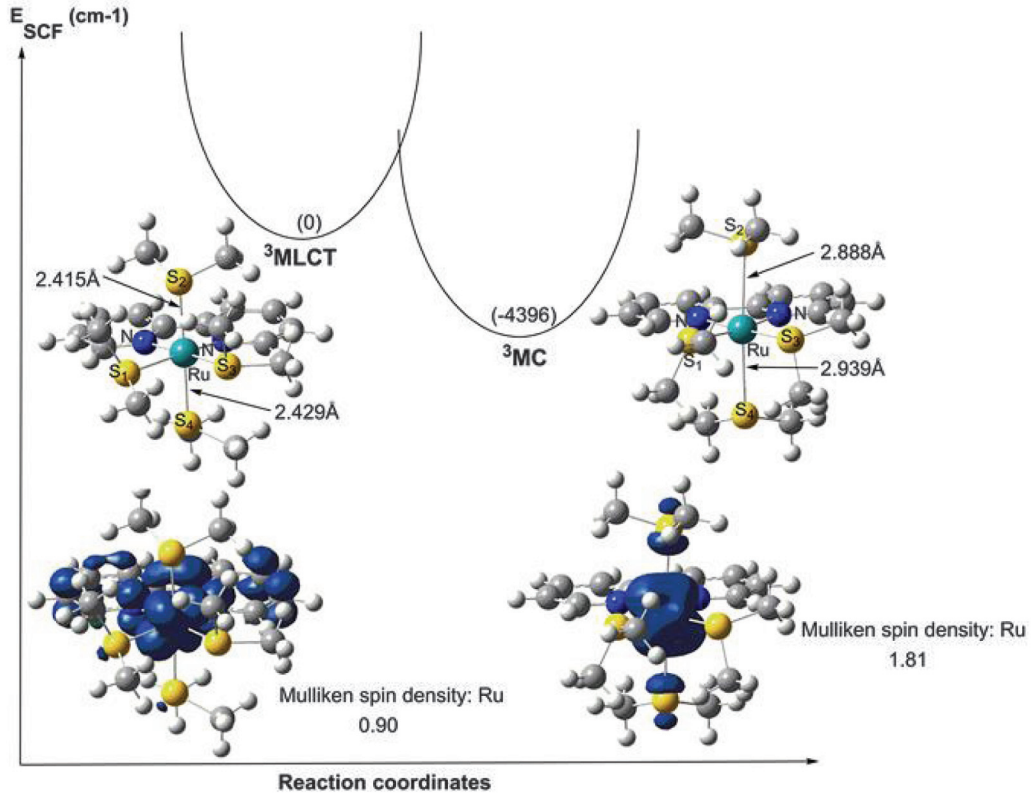

Fig. 14. Successive 405 nm irradiations of 8.4 × 10^{-4} mol L^{-1} $[Ru(NCCH_3)_4bpy]^{2+}$ in a 77 K 4:1 ethanol–methanol glass. Spectral accumulations required 1 m irradiation each; arrows indicate increasing photolysis time. (*a*) The sample was irradiated with the unfiltered output of a 50 mW diode laser for 3 m between each spectral accumulation (seven irradiation periods); (*b*) the sample was irradiated using a 50% neutral density filter in the 50 mW diode laser excitation beam. Irradiation periods were for 360 s between the first four spectral accumulations and 180 s between the last two. The arrows indicate the direction of the spectroscopic changes with irradiation.

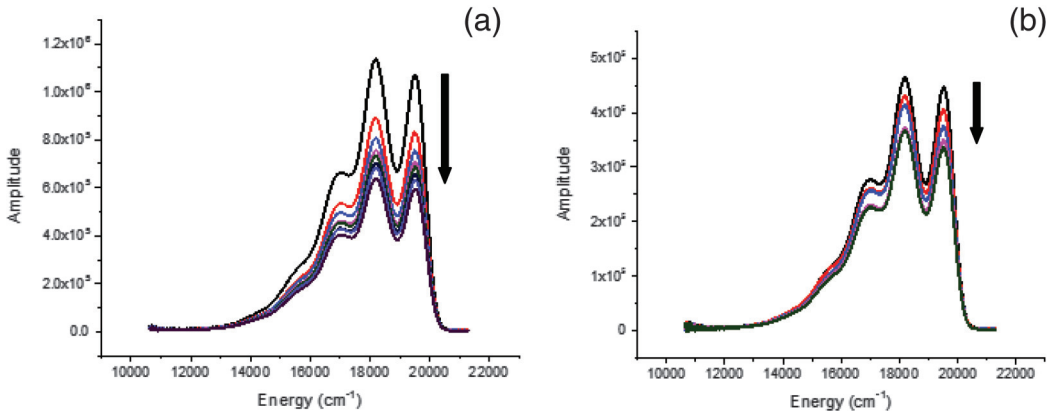

the spectra were acquired using 1 min irradiation periods with the 405 nm diode laser for excitation. The experiments were performed in sequence from 77 to 107 K in the cryostat. There is significant photodecomposition in these experiments even with the pulsed dye laser (4 ns pulse width) although not as dramatic as found for irradiations with the 405 nm diode laser. The changes in spectra and lifetimes are larger at the higher temperatures.

(*ii*) We attempted to minimize the photochemical effects in the experiments summarized at the bottom of Table 5. There were no intermediate periods of irradiation and we used 410 nm pulsed laser excitation. We also began these experiments with the sample at 107 K in the cryostat and the experiments were performed in sequence from 107 to 77 K.

We have attempted to characterize the minor (≈15%) and short-lived emission component. This component has been present to nearly the same extent in several different sample preparations, in two different solvent glasses and it appears to be independent of the rate of sample cooling. Tables 3 and 4 indicate that its contribution to the overall emission is excitation wavelength independent and that there is no particular region of the emission spectrum in which its contribution is different from that of the dominant component. However, since this is a minor component,

Fig. 15. Variation of the quantum yield for the decrease of $[Ru(NCCH_3)bpy]^{2+}$ emission intensity with the extent of irradiation at different incident light intensities (I_o) in an ethanol–methanol glass. Irradiations at 50 mW 405 nm diode laser with 50% (I_o/2) and 90% (I_o/10) neutral density filters (I_o is the diode laser output). The relative number of photons absorbed is calculated from I_a(rel) × t_{irrad} × f (where f = 1 (for no neutral density filter), 0.5, or 0.10, t_{irrad} is the total time of irradiation, and I_a(rel) = $I_a(f)/I_a(f = 1)$.

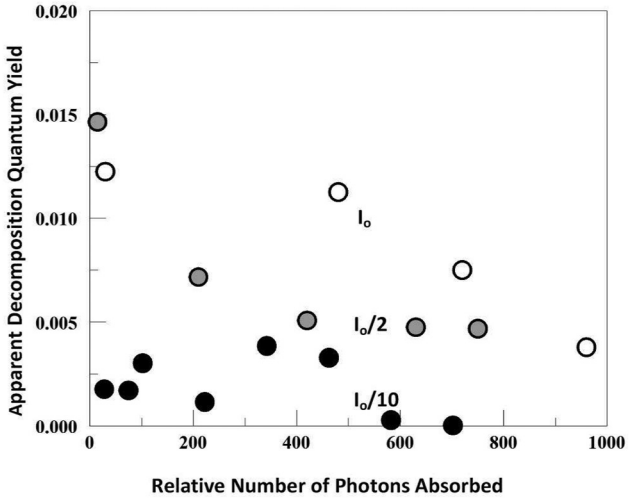

Fig. 16. Emission decay of $[Ru(NCCH_3)_4bpy]^{2+}$ (2.0×10^{-4} M) at 77 K in a 4:1 ethanol–methanol glass for 405 nm pulsed excitation monitored at 510 nm. The two-exponential fit (black) and original signal (blue) are indistinguishable; residuals are in red. Color in online version only.

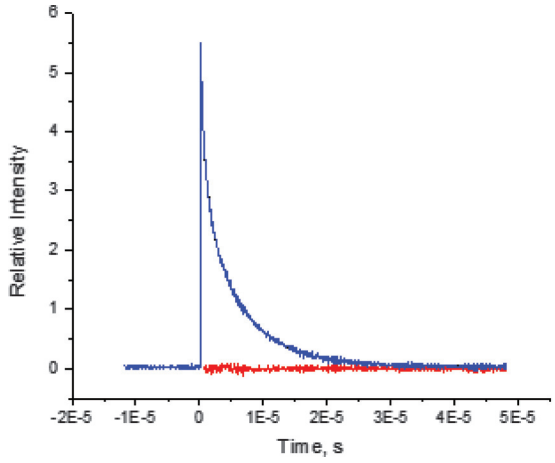

its spectroscopic signatures might be difficult to detect. Nevertheless, these observations suggest that the species giving rise to this emission must have absorption and emission spectra that are very similar to that of the dominant chromophore. One hypothesis that would be consistent with the observations is that since the acetonitrile ligand is a relatively poor σ-donor, and thus a poor ligand for Ru(III), there could be a distribution of ^{3}MLCT species in the frozen solutions with slightly different Ru–$NCCH_3$ bond lengths and decay lifetimes. This possibility would imply that the mean ^{3}MLCT excited state emission decay rate constant (weighted by the respective percentages) is between about 2.4×10^5 s^{-1}, for the lowest intensity irradiations in Table 5, and about 3×10^5 s^{-1}, for the median values found in other experiments.

Overall, the extent of photodecomposition in these experiments does not appear to significantly influence our observations on the lifetimes of the $[Ru(NCCH_3)_4bpy]^{2+}$ complex. The temperature dependencies of two apparent components are very small; in a simple semiclassical[19] reactant/product formulation, $E_a(1) \approx 80$ cm^{-1} and $E_a(2) \approx 170$ cm^{-1} and $\kappa_{el}\nu_{nu} \approx 4.6 \times 10^6$ and 3.1×10^6 s^{-1}, respectively, for these components. In the absence of competing internal conversion processes, the measured lifetime, $\tau_{obs} = 1/k_{obs}$, is a function of the radiative and non-radiative rate constants,

$$1/\tau_{obs} \approx k_r + k_{nr} \quad (13)$$

The radiative rate constant should be temperature independent and at sufficiently low temperature, k_{nr} should approach a temperature-independent limit,[74] so a small value of E_a is expected and it is consistent with the trapping of most of the excitation energy in the local potential energy minimum (see Fig. 9). The fractional contributions of the two components to the observed emission can be estimated from eq. 12, and most of the change in emission intensity arises from the more strongly temperature-dependent contributions from component 2, which decreases from about 85% at 77 K to about 55% at 107 K. Since this behavior is nearly independent of the extent of photolysis or the sequence in which the temperature is changed, it cannot be attributed to contributions arising from the appreciable increase in photochemical products as the temperature is increased. However, this effect could arise from a broadening of the distribution of ^{3}MLCT species with slightly different bond lengths with increasing temperature.

The 77 K emission quantum yield of $[Ru(NCCH_3)_4bpy]^{2+}$

The ANDOR Newton detector/liquid light guide combination that we used for spectroscopic determinations has no response to light wavelengths less than or equal to 395 nm. As a consequence, we were only able to obtain partial 90 K absorption spectra for this complex, but the ambient absorptivity at 405 nm was in good agreement with that obtained with a standard spectrophotometer. At 405 nm, we found the 90 K absorptivity for $[Ru(NCCH_3)_4bpy]^{2+}$ to be 4960 M^{-1} cm^{-1} compared with 7100 M^{-1} cm^{-1} for $[Ru(bpy)_3]^{2+}$. Based on this, the ratio of the integrated emission intensities of these complexes for the same irradiation time, and eq. 1, we find an emission quantum yield of 0.47 ± 0.04 for the $[Ru(NCCH_3)_4bpy]^{2+}$ complex.

Conclusions

We initiated this study because the very similar absorption and emission spectra of $[Ru(NCCH_3)_4bpy]^{2+}$ and $[Ru([14]aneS_4)bpy]^{2+}$ but very different lifetimes and photochemistry seemed to implicate a lower energy ^{3}MC than ^{3}MLCT excited state in the latter but not in the former. The computational modeling confirms that the lowest energy excited state of $[Ru([14]aneS_4)bpy]^{2+}$ is metal centered, but it also indicates that this is the case for the $[Ru(NCCH_3)_4bpy]^{2+}$ complex. The differences in photochemistry and photophysics appear to arise largely from the large differences in the respective energies for their ^{3}MLCT/^{3}MC potential energy surface crossings, differences that arise from the large differences in ^{3}MC excited-state Ru–ligand distortions. The observed differences in 77 K excited-state lifetimes can be qualitatively rationalized in terms of an electron transfer analogy: the reorganizational energies for intramolecular electron transfer, bpy^{-} to Ru^{III}, are very different. Thus, the excited-state behavior of these two complexes is analogous to the classical patterns of the dependence of electron transfer rate constants on variations metal–ligand bond lengths,[14,24] with the rate constants for the transitions from the initial (or reactant) state to the final (or product) state decreasing as the bond length (and (or) bond angle) differences of these states increases, provided their energy differences are comparable; the calculations indicate that ^{3}MLCT and

Table 3. 77 K lifetime measurements of $[Ru(NCCH_3)_4bpy]^{2+}$ (2.0×10^{-4} mol L^{-1}) with different excitation wavelengths in 4:1 ethanol–methanol solvent (monitored at 510 nm).

	Single exponential fit		Double exponential fit[a]				
Excitation wavelength (nm)	Lifetime (μs)	Initial amplitude	Lifetime 1 (μs)	Initial amplitude 1	Lifetime 2 (μs)	Initial amplitude 2	% of 2 in emission[b]
375	4.7	3.3	1.06	2.2	6.2	2.4	87
380	4.9	3.9	1.00	2.7	6.5	3.0	88
385	5.1	4.1	1.12	2.7	6.7	3.0	87
390	5.2	4.3	1.06	2.9	6.8	3.2	88
395	5.1	3.9	1.12	2.4	6.6	2.9	89
400	5.3	4.0	1.06	2.4	6.6	3.1	89
405	5.1	3.7	1.06	2.2	6.4	2.9	89
410	4.6	2.3	1.17	1.4	6.2	1.6	86
415	4.5	1.9	1.17	1.2	6.1	1.3	85

[a]Fast decay labeled "1"; slow decay labeled "2".
[b]A = initial amplitude; emission percentage = $100 \times [A(2)\tau(2)/(A(2)\tau(2) + A(1)\tau(1))]$.

Table 4. 77 K lifetime measurements of $[Ru(NCCH_3)_4bpy]^{2+}$ (1.8×10^{-4} mol L^{-1}) with different monitoring wavelengths in butyronitrile solvent (405 nm excitation).

	Single exponential fit		Double exponential fit[a]				
Wavelength monitored (nm)	Lifetime (μs)	Initial amplitude	Lifetime 1 (μs)	Initial amplitude 1	Lifetime 2 (μs)	Initial amplitude 2	% of 2 in emission[b]
510	5.0	3.9	1.02	3.2	7.0	2.8	86
520	5.3	4.3	0.98	3.9	7.5	3.1	86
530	5.2	4.0	1.03	3.2	7.2	2.9	86
540	5.3	3.9	1.04	2.9	7.1	2.9	87
550	5.2	3.7	1.08	2.7	7.0	2.6	86
560	5.1	3.5	1.11	2.3	6.9	2.6	87
570	5.0	2.9	1.23	1.9	6.8	2.1	86
580	4.8	2.2	1.20	1.5	6.7	1.5	85
590	4.9	2.1	1.35	1.3	6.7	1.5	85
600	4.7	1.8	1.22	1.1	6.4	1.3	86

[a]Fast decay labeled "1"; slow decay labeled "2".
[b]A = initial amplitude; emission percentage = $100 \times [A(2)\tau(2)/(A(2)\tau(2) + A(1)\tau(1))]$.

Table 5. Temperature dependence of the emission decay lifetime for $[Ru(NCCH_3)_4bpy]^{2+}$ in butyronitrile glasses (temperatures were varied using samples in a cryostat).

	Double exponential fit[a]					
Temperature (K)	Lifetime 1 (μs)	Initial amplitude 1	Lifetime 2 (μs)	Initial amplitude 2	Relative amplitude (A1, A2) (%)[b]	% of 2 in emission[b]
77[c]	1.07	2.9	6.4	2.8	51, 49	85
87[c]	1.02	3.0	5.0	2.2	58, 42	78
97[c]	0.81	2.8	3.8	1.1	72, 28	64
107[c]	0.50	2.1	2.5	0.49	81, 19	52
77[d]	1.43	0.83	6.1	0.77	52, 48	80
77[e]	1.02	4.5	7.9	3.8	54, 46	86
87[e]	0.84	4.8	5.5	3.6	57, 43	83
97[e]	0.75	5.4	3.9	2.5	69, 31	69
107[e]	0.66	4.8	3.3	1.2	80, 20	55

[a]Fast decay labelled "1", slow decay labelled "2".
[b]A = initial amplitude; emission percentage = $100 \times (\int(A2)e^{-\tau(2)t}dt)/(\int(A2)e^{-\tau(2)t}dt + \int(A1)e^{-\tau(1)t}dt)$.
[c]Temperature ramped from 77 to 107 K; sample photolyzed for 3 min between lifetime measurements.
[d]Lifetime measurements using a 10% neutral density filter.
[e]Temperature ramped from 107 to 77 K; no intermediate photolysis.

^{3}MC PE minima differ by about 3700 ± 100 cm^{-1} for these complexes.

The observations reported here indicate that the ^{3}MLCT/^{3}MC configurational mixing is very small: (*i*) the emission of the $[Ru([14]aneS_4)bpy]^{2+}$ has relatively well-resolved vibronic components[32] despite its weak emission and a calculated ^{3}MLCT/^{3}MC crossing point that is very close in energy to the ^{3}MLCT potential energy minimuim, (*ii*) the $[Ru(NCCH_3)_4bpy]^{2+}$ complex emission is very strong, and (*iii*) the electronic configurations change abruptly in the calculated crossing regions. Furthermore, our studies indicate that the excited state ^{3}MLCT/^{3}MC crossing energies can be manipulated using conventional stereochemical constraints that restrict the extent of metal–ligand distortions.

The more careful examination of the low-temperature emission properties of the $[Ru(NCCH_3)_4bpy]^{2+}$ complex has also revealed some unexpected features: (*i*) the 77 K emission quantum yield is large (0.47 ± 0.04), (*ii*) the emission decay appears to be bi- or multiphasic, (*iii*) the two emission components appear to have different, but very small, temperature dependencies, and (*iv*) two-photon photodecomposition is a problem even at low temperatures. The large emission quantum yield is surprising in view of the calculated lower energy of the ^{3}MC than the ^{3}MLCT excited

state. In fact, most of the 77 K spectroscopic properties of this complex are typical of Ru-bpy chromophores. However, the above arguments imply that its radiative rate constant is approximately in the range of $k_r = \phi_{em} \times k_{obs} \approx (0.6–0.8) \times 10^5$ s^{-1}. This can be compared with a value of $k_r = 0.7 \times 10^5$ s^{-1} for $[Ru(bpy)_3]^{2+}$.[70] Since k_r is expected to increase strongly as the excited-state energy increases,[75] and since $[Ru(NCCH_3)_4bpy]^{2+}$ emits at about 2000 cm^{-1} higher energy than $[Ru(bpy)_3]^{2+}$, the comparable inferred value of k_r for the former implies a somewhat inefficient population of the emitting state, similar to the behavior of $[Ru(L)_5MDA]^{2+}$ complexes,[34] and this would be consistent with some relaxation pathways leading to the lower energy ^{3}MC state proposed above. A conventional excited-state relaxation cascade through successive states could result in a large transient population of a high-energy excited state with a well-defined local potential energy minimum, and this appears to be the best current overall interpretation of the photophysics of the $[Ru(NCCH_3)_4bpy]^{2+}$ complex. While a strong emission from any but the lowest energy excited state is unusual among transition metal complexes, the recent work of Hauser and co-workers indicates that even in complexes with Ru-substituted-bpy chromophores in which the lowest energy excited state is a ^{3}MC state, a high percentage of a higher energy ^{3}MLCT excited state is transiently populated in ambient solutions.[76] For one of these complexes, $[Ru(6\text{-}Me\text{-}bpy)_3]^{2+}$, these authors calculated that the ^{3}MC state is 300 cm^{-1} lower in energy than the ^{3}MLCT state with transient lifetimes of 450 and 1.6 ps, respectively, found for them in ambient solution. This complex is known to emit at 77 K with an emission maximum of 17 000 cm^{-1}, $\phi_{em} = 0.097$, and $k_r = 2.4 \times 10^4$ s^{-1}.[10] This is qualitatively similar to the related observations on $[Ru(NCCH_3)_4bpy]^{2+}$, but the detailed interpretation is a little more ambiguous, since the chromophores are not the same. However, there are now several different complexes in which a MLCT 77 K emission occurs from a complex in which $E(^3MC) < E(^3MLCT)$. There will undoubtedly be more.

Supplementary material

Supplementary material (computational details) for this paper is available on the journal web site at http://nrcresearchpress.com/doi/suppl/10.1139/cjc-2014-0155.

Acknowledgements

We have depended on Barry Lever for “final” words about transition metal spectroscopy for many years. His work and comments have been consistently informative and stimulating. This work was funded in part by the Division of Chemical Sciences, Geosciences, and Biosciences, Office of Basic Energy Sciences, of the US Department of Energy through grant DE-FG02-09ER16120.

References

(1) Graetzel, M. *Inorg. Chem.* **2005**, *44*, 6841. doi:10.1021/ic0508371.
(2) Graetzel, M.; Moser, J.-E. In *Electron Transfer in Chemistry*, Vol. 5; Balzani, V., Ed.; Wiley-VCH: Weinheim, Germany, 2001.
(3) Alstrum-Acevedo, J. H.; Brennaman, M. K.; Meyer, T. J. *Inorg. Chem.* **2005**, *44*, 6802. doi:10.1021/ic050904r.
(4) Balzani, V.; Credi, A.; Venturi, M. *Coord. Chem. Rev.* **1998**, *171*, 3. doi:10.1016/S0010-8545(98)90005-4.
(5) Balzani, V.; Juris, A.; Venturi, M.; Campagna, S.; Serroni, S. *Chem. Rev.* **1996**, *96*, 759. doi:10.1021/cr941154y.
(6) Balzani, V.; Scandola, F. *Supramolecular Photochemistry*; Horwood: Chichester, UK, 1991.
(7) Barbara, P. F.; Meyer, T. J.; Ratner, M. *J. Phys. Chem.* **1996**, *100*, 13148. doi:10.1021/jp9605663.
(8) Lewis, N. S. *Inorg. Chem.* **2005**, *44*, 6900. doi:10.1021/ic051118p.
(9) Lewis, N. S.; Nocera, D. G. *Proc. Natl. Acad. Sci. U.S.A.* **2006**, *103*, 15729. doi:10.1073/pnas.0603395103.
(10) Fabian, R. H.; Klassen, D. M.; Sonntag, R. W. *Inorg. Chem.* **1980**, *19*, 1977. doi:10.1021/ic50209a029.
(11) Ondersma, J. W.; Hamann, T. W. *Coord. Chem. Rev.* **2013**, *257*, 1533. doi:10.1016/j.ccr.2012.09.010.
(12) Manbeck, G. F.; Brewer, K. J. *Coord. Chem. Rev.* **2013**, *257*, 1660. doi:10.1016/j.ccr.2012.10.019.
(13) Balzani, V. *Electron Transfer in Chemistry*, Vols. 1–5; Wiley-VCH: Weinheim, Germany, 2001.
(14) Marcus, R. A. *Discuss. Faraday Soc.* **1960**, *29*, 21. doi:10.1039/df9602900021.
(15) Marcus, R. A. *Annu. Rev. Phys. Chem.* **1964**, *15*, 155. doi:10.1146/annurev.pc.15.100164.001103.
(16) Marcus, R. A. *Phys. Chem. Chem. Phys.* **2012**, *14*, 13729. doi:10.1039/c2cp90116a.
(17) Newton, M. D. In *Electron Transfer In Chemistry*, Vol. 1; Balzani, V., Ed.; Wiley-VCH: Weinheim, Germany, 2001.
(18) Newton, M. D. In *Comprehensive Coordination Chemistry II*, Vol. 2; McCleverty, J. A.; Meyer, T. J., Eds.; Elsevier, 2004.
(19) Newton, M. D.; Sutin, N. *Annu. Rev. Phys. Chem.* **1984**, *35*, 437. doi:10.1146/annurev.pc.35.100184.002253.
(20) Newton, M. D. *Chem. Rev.* **1991**, *91*, 767. doi:10.1021/cr00005a007.
(21) Newton, M. D. *J. Phys. Chem.* **1991**, *95*, 30. doi:10.1021/j100154a010.
(22) Newton, M. D. *J. Electroanal. Chem.* **1997**, *438*, 3. doi:10.1016/S0022-0728(96)05025-5.
(23) Newton, M. D. *Adv. Chem. Phys.* **1999**, *106*, 303. doi:10.1002/9780470141656.ch7.
(24) Endicott, J. F. In *Comprehensive Coordination Chemistry II*, 2nd ed.; Vol. 7; McCleverty, J.; Meyer, T. J., Eds.; Pergamon: Oxford, UK, 2003.
(25) Hupp, J. T.; Williams, R. T. *Acc. Chem. Res.* **2001**, *34*, 808. doi:10.1021/ar9602720.
(26) Maruszewski, K.; Bajdor, K.; Strommen, D. P.; Kincaid, J. R. *J. Phys. Chem.* **1995**, *99*, 6286. doi:10.1021/j100017a006.
(27) Myers, A. B.; Mathies, R. A.; Tannor, D. J.; Heller, E. J. *J. Chem. Phys.* **1982**, *77*, 3857. doi:10.1063/1.444339.
(28) Thompson, D. G.; Schoonover, J. R.; Timpson, C. J.; Meyer, T. J. *J. Phys. Chem. A* **2003**, *107*, 10250. doi:10.1021/jp0303366.
(29) Chen, Y.-J.; Xie, P.; Endicott, J. F. *J. Phys. Chem. A* **2004**, *108*, 5041. doi:10.1021/jp0497817.
(30) Odongo, O. S.; Heeg, M. J.; Chen, Y.-J.; Xie, P.; Endicott, J. F. *Inorg. Chem.* **2008**, *47*, 7493. doi:10.1021/ic7024473.
(31) Xie, P.; Chen, Y.-J.; Uddin, M. J.; Endicott, J. F. *J. Phys. Chem. A* **2005**, *109*, 4671. doi:10.1021/jp050263l.
(32) Lord, R. L.; Allard, M. M.; Thomas, R. A.; Odongo, O. S.; Schlegel, H. B.; Chen, Y.-J.; Endicott, J. F. *Inorg. Chem.* **2013**, *52*, 1185. doi:10.1021/ic300935k.
(33) Shaw, G. B.; Grant, C. D.; Shirota, H.; Castner, E. W., Jr.; Meyer, G. J.; Chen, L. X. *J. Am. Chem. Soc.* **2007**, *129*, 2147. doi:10.1021/ja067271f.
(34) Tsai, C.-N.; Tian, Y.-H.; Shi, X.; Lord, R. L.; Luo, D.-W.; Schlegel, H. B.; Endicott, J. F.; Chen, Y.-J. *Inorg. Chem.* **2013**, *52* (17), 9774. doi:10.1021/ic4016614.
(35) Wagenknecht, P. S.; Ford, P. C. *Coord. Chem. Rev.* **2011**, *255*, 591. doi:10.1016/j.ccr.2010.11.016.
(36) Ciofini, I.; Daul, C. A.; Adamo, C. *J. Phys. Chem. A* **2003**, *107*, 11182. doi:10.1021/jp0307607.
(37) Alary, F.; Heully, J.-L.; Bijeire, L.; Vicendo, P. *Inorg. Chem.* **2007**, *46*, 3154. doi:10.1021/ic062193i.
(38) Abrahamsson, M.; Lundqvist, M. J.; Wolpher, H.; Johansson, O.; Eriksson, L.; Bergquist, J.; Rasmussen, T.; Becker, H.-C.; Hammarström, L.; Norrby, P.-O.; Åkermark, B.; Persson, P. *Inorg. Chem.* **2008**, *47*, 3540. doi:10.1021/ic7019457.
(39) Alary, F.; Boggio-Pasqua, M.; Heully, J.-L.; Marsden, C. J.; Vicendo, P. *Inorg. Chem.* **2008**, *47*, 5259. doi:10.1021/ic800246t.
(40) Salassa, L.; Garino, C.; Salassa, G.; Gobetto, R.; Nervi, C. *J. Am. Chem. Soc.* **2008**, *130*, 9590. doi:10.1021/ja8025906.
(41) Borg, O. A.; Godinho, S. S. M. C.; Lundqvist, M. J.; Lunell, S.; Persson, P. *J. Phys. Chem. A* **2008**, *112*, 4470. doi:10.1021/jp8000702.
(42) Salassa, L.; Garino, C.; Salassa, G.; Nervi, C.; Gobetto, R.; Lamberti, C.; Gianolio, D.; Bizzarri, R.; Sadler, P. J. *Inorg. Chem.* **2009**, *48*, 1469. doi:10.1021/ic8015436.
(43) Jakubikova, E.; Chen, W.; Dattelbaum, D. M.; Rein, F. N.; Rocha, R. C.; Martin, R. L.; Batista, E. R. *Inorg. Chem.* **2009**, *48*, 10720. doi:10.1021/ic901477m.
(44) Heully, J.-L.; Alary, F.; Boggio-Pasqua, M. *J. Chem. Phys.* **2009**, *131*, 184308. doi:10.1063/1.3254196.
(45) Sun, Y.; El Ojaimi, M.; Hammitt, R.; Thummel, R. P.; Turro, C. *J. Phys. Chem. B* **2010**, *114* (45), 14664. doi:10.1021/jp102613n.
(46) Dixon, I. M.; Alary, F.; Heully, J.-L. *Dalton Trans.* **2010**, *39*, 10959. doi:10.1039/c0dt00563k.
(47) Jakubikova, E.; Martin, R. L.; Batista, E. R. *Inorg. Chem.* **2010**, *49*, 2975. doi:10.1021/ic902504y.
(48) Gottle, A. J.; Dixon, I. M.; Alary, F.; Heully, J.-L.; Boggio-Pasqua, M. *J. Am. Chem. Soc.* **2011**, *133*, 9172. doi:10.1021/ja201625b.
(49) Scarborough, C. C.; Wieghardt, K. *Inorg. Chem.* **2011**, *50*, 9773. doi:10.1021/ic2005419.
(50) Lebon, E.; Bastin, S.; Sutra, P.; Vendier, L.; Piau, R. E.; Dixon, I. M.; Boggio-Pasqua, M.; Alary, F.; Heully, J.-L.; Igau, A. *Chem. Commun.* **2012**, *48*, 741. doi:10.1039/c1cc15737j.
(51) Oesterman, T.; Abrahamsson, M.; Becker, H.-C.; Hammarstroem, L.; Persson, P. *J. Phys. Chem. A* **2012**, *116* (3), 1041. doi:10.1021/jp207044a.
(52) Scarborough, C. C.; Sproules, S.; Doonan, C. J.; Hagen, K. S.; Weyhermüller, T.; Wieghardt, K. *Inorg. Chem.* **2012**, *51* (12), 6969. doi:10.1021/ic300882r.
(53) Camilo, M. R.; Cardoso, C. R.; Carlos, R. M.; Lever, A. B. P. *Inorg. Chem.* **2014**, *53* (7), 3694. doi:10.1021/ic5000205.
(54) Petroni, A.; Slep, L. D.; Etchenique, R. *Inorg. Chem.* **2008**, *47*, 951. doi:10.1021/ic7018204.

(55) Adams, H.; Amado, A. M.; Felix, V.; Mann, B. E.; Antelo-Martinez, J.; Newell, M.; Ribeiro-Claro, P. J. A.; Spey, S. E.; Thomas, J. A. *Chem. Eur. J.* **2005**, *11*, 2031. doi:10.1002/chem.200400693.
(56) Parr, R. G.; Yang, W. *Density-Functional Theory of Atoms and Molecules*; Oxford University Press: New York, 1989.
(57) Frisch, M. J.; Trucks, G. W.; Schlegel, H. B.; Scuseria, G. E.; Robb, M. A.; Cheeseman, J. R.; Scalmani, G.; Barone, V.; Mennucci, B.; Petersson, G. A.; Nakatsuji, H.; Caricato, M.; Li, X.; Hratchian, H. P.; Izmaylov, A. F.; Bloino, J.; Zheng, G.; Sonnenberg, J. L.; Hada, M.; Ehara, M.; Toyota, K.; Fukuda, R.; Hasegawa, J.; Ishida, M.; Nakajima, T.; Honda, Y.; Kitao, O.; Nakai, H.; Vreven, T.; Montgomery, J. A.; Peralta, J. E.; Ogliaro, F.; Bearpark, M.; Heyd, J. J.; Brothers, E.; Kudin, K. N.; Staroverov, V. N.; Kobayashi, R.; Normand, J.; Raghavachari, K.; Rendell, A.; Burant, J. C.; Iyengar, S. S.; Tomasi, J.; Cossi, M.; Rega, N.; Millam, J. M.; Klene, M.; Knox, J. E.; Cross, J. B.; Bakken, V.; Adamo, C.; Jaramillo, J.; Gomperts, R.; Stratmann, R. E.; Yazyev, O.; Austin, A. J.; Cammi, R.; Pomelli, C.; Ochterski, J. W.; Salvador, P.; Dannenberg, J. J.; Dapprich, S.; Parandekar, P. V.; Mayhall, N. J.; Daniels, A. D.; Farkas, O.; Foresman, J. B.; Ortiz, J. V.; Cioslowski, J.; Fox, D. J. *Gaussian Development Version, Revision H.20 ed.*; Gaussian, Inc.: Wallingford, CT, 2010.
(58) Perdew, J. P. *Phys. Rev. B* **1986**, *33*, 8822. doi:10.1103/PhysRevB.33.8822.
(59) Perdew, J. P.; Burke, K.; Wang, Y. *Phys. Rev.* **1996**, *54*, 16533. doi:10.1103/PhysRevB.54.16533.
(60) Andrae, D.; Haussermann, U.; Dolg, M.; Stoll, H.; Preuss, H. *Theor. Chim. Acta* **1990**, *77* (2), 123. doi:10.1007/BF01114537.
(61) Dunning, T. H., Jr.; Hay, P. J. In *Modern Theoretical Chemistry*, Vol. 3; Schaefer, H. F. III, Ed.; Plenum: New York, 1976.
(62) Igelmann, G.; Stoll, H.; Preuss, H. *Mol. Phys.* **1988**, *65* (6), 1321. doi:10.1080/00268978800101811.
(63) Hariharan, P. C.; Pople, J. A. *Theor. Chim. Acta* **1973**, *28*, 213. doi:10.1007/BF00533485.
(64) Francl, M. M.; Petro, W. J.; Hehre, W. J.; Binkley, J. S.; Gordon, M. S.; DeFrees, D. J.; Pople, J. A. *J. Chem. Phys.* **1982**, *77*, 3654. doi:10.1063/1.444267.
(65) Marenich, A. V.; Cramer, C. J.; Truhlar, D. G. *J. Phys. Chem. B* **2009**, *113*, 6378. doi:10.1021/jp810292n.
(66) Dennington, R.; Keith, T.; Millam, J. M. *GaussView, Version 5*; Semichem, Inc.: Shawnee Mission, KS, 2009.
(67) Schlegel, H. B. The Mathematica notebook for optimization on a seam is available free of charge at http//chem.wayne.edu/schlegel/Software.html.
(68) Allard, M. M.; Odongo, O. S.; Lee, M. M.; Chen, Y.-J.; Endicott, J. F.; Schlegel, H. B. *Inorg. Chem.* **2010**, *49*, 6840. doi:10.1021/ic100202h.
(69) Endicott, J. F.; Chen, Y.-J.; Xie, P. *Coord. Chem. Rev.* **2005**, *249*, 343. doi:10.1016/j.ccr.2004.08.013.
(70) Demas, J. N.; Crosby, G. A. *J. Am. Chem. Soc.* **1971**, *93*, 2841. doi:10.1021/ja00741a003.
(71) Wilson, R. B.; Solomon, E. I. *J. Am. Chem. Soc.* **1980**, *102*, 4085. doi:10.1021/ja00532a018.
(72) Hakamata, K.; Urushiyama, A.; Kupka, H. *J. Phys. Chem.* **1981**, *85*, 1983. doi:10.1021/j150614a007.
(73) Creutz, C.; Chou, M.; Netzel, T. L.; Okumura, M.; Sutin, N. *J. Am. Chem. Soc.* **1980**, *102*, 1309. doi:10.1021/ja00524a014.
(74) Englman, R.; Jortner, J. *Mol. Phys.* **1970**, *18*, 145. doi:10.1080/00268977000100171.
(75) Birks, J. B. *Photophysics of Aromatic Molecules*; Wiley-Interscience: New York, 1970.
(76) Sun, Q.; Mosquera-Vazquez, S.; Daku, L. M. L.; Guénée, L.; Goodwin, H. A.; Vauthey, E.; Hauser, A. *J. Am. Chem. Soc.* **2013**, *135* (37), 13660. doi:10.1021/ja407225t.